

Aeronomy of extra-solar giant planets at small orbital distances

Roger V. Yelle

Department of Planetary Sciences, University of Arizona, Tucson, AZ 85721, USA

Received 20 August 2003; revised 12 February 2004

Available online 24 April 2004

Abstract

One-dimensional aeronomical calculations of the atmospheric structure of extra-solar giant planets in orbits with semi-major axes from 0.01 to 0.1 AU show that the thermospheres are heated to over 10,000 K by the EUV flux from the central star. The high temperatures cause the atmosphere to escape rapidly, implying that the upper thermosphere is cooled primarily by adiabatic expansion. The lower thermosphere is cooled primarily by radiative emissions from H_3^+ , created by photoionization of H_2 and subsequent ion chemistry. Thermal decomposition of H_2 causes an abrupt change in the composition, from molecular to atomic, near the base of the thermosphere. The composition of the upper thermosphere is determined by the balance between photoionization, advection, and H^+ recombination. Molecular diffusion and thermal conduction are of minor importance, in part because of large atmospheric scale heights. The energy-limited atmospheric escape rate is approximately proportional to the stellar EUV flux. Although escape rates are large, the atmospheres are stable over time scales of billions of years. © 2004 Elsevier Inc. All rights reserved.

Keywords: Extra-solar planets; Aeronomy; Atmospheric escape

1. Introduction

Radial velocity observations and measurements of the dimming of light during transit events show that HD209458b is a Jupiter-like planet orbiting a Sun-like star (Charbonneau et al., 2000, 2002; Henry et al., 2000). Spectroscopic observations during the transit have detected the NaI D lines and the H Ly α line in absorption (Charbonneau et al., 2002; Vidal-Madjar et al., 2003), providing the first opportunity to observationally constrain the structure of an Extra-solar Giant Planet (EGP) atmosphere. The spectroscopic detections to date probe different regions of the atmosphere. The apparent size of HD209458b, when viewed in the NaI lines, is only slightly larger than the apparent size of the planet at nearby wavelengths, suggesting that the observations probe a region in the troposphere of the planet, not too far from the cloud tops (Charbonneau et al., 2002). The apparent size of HD209458b in the H Ly α line is several planetary radii, implying that these observations probe the upper-most regions of an extended atmosphere (Vidal-Madjar et al., 2003). Numerous studies of the lower atmospheres of EGPs have been carried out (cf. Sudarsky et al., 2003, and references therein);

the first comprehensive investigation of the physical state of EGP upper atmospheres is presented below.

The surprisingly large extent of the H cloud detected by Vidal-Madjar et al. (2003) implies that the scale height of the upper atmosphere is a significant fraction of a planetary radius. Yet, the skin temperature of an EGP at 0.05 AU is expected to be approximately 750 K (Goukenleuque et al., 2000; Seager et al., 2000; Sudarsky et al., 2003) and the gravitational acceleration of HD209458b is $\sim 900 \text{ cm s}^{-2}$, implying a scale height of $\sim 700 \text{ km}$, a value far too small to explain the observed H cloud. Thus, the existence of an extended H cloud implies that the upper atmosphere of HD209458b is at a much higher temperature than the lower atmosphere. Moreover, as on Jupiter, H_2 , not H, is the thermodynamically stable form of hydrogen at the temperatures and pressure of EGP atmospheres considered to date (Goukenleuque et al., 2000; Sudarsky et al., 2003). The existence of an extended H cloud implies either that the upper atmosphere is much hotter than the skin temperature, or that H is produced at a rapid rate by non-equilibrium processes. This paper investigates whether absorption of stellar EUV radiation in the upper atmosphere of an EGP can lead to the conditions implied by Vidal-Madjar et al.'s measurements. To this end, physical models of EGP upper atmospheric structure are constructed using techniques de-

E-mail address: yelle@lpl.arizona.edu.

veloped in studies of Solar-System aeronomy. An improved understanding of the upper atmospheric structure of EGPs may also aid in their detection and characterization, by, for example, predicting other emission or absorption features or identifying preferred wavelength bands for extra-solar planet searches. Finally, the escape rate of the atmosphere is determined by conditions in the thermosphere; thus, the evolution of extra-solar planets may depend on their aeronomy (Mayor and Queloz, 1995; Burrows and Lunine, 1995; Guillot et al., 1996; Vidal-Madjar et al., 2003; Liang et al., 2003; Lammer et al., 2003).

Our investigation of the aeronomy of extra-solar planets is grounded in studies of Jupiter. Unfortunately, our understanding of the structure of Jupiter's thermosphere and ionosphere is not as robust as we would like. Measurements of the peak electron density in the jovian ionosphere are often a factor of 10 less and occur at an altitude several scale heights above that predicted by photochemical models (McConnell and Majeed, 1987). Measurements by the Galileo spacecraft indicate a complex situation with large temporal and spatial variations that have yet to be adequately interpreted (Majeed et al., 1999). Suggestions for the discrepancies include a non-thermal H_2 vibrational distribution (Majeed et al., 1991; Cravens, 1987) and thermospheric winds coupled with specific magnetic field geometries (McConnell and Majeed, 1987; Matcheva et al., 2001), but these have yet to be verified and the problem is still without a clear resolution (Yelle and Miller, 2004). Also, the thermospheric temperature on Jupiter is much higher than predicted by aeronomical models based on solar energy input and the heat source has yet to be unambiguously identified (Yelle and Miller, 2004). The high temperatures may be due to dissipation of buoyancy or acoustic waves (Young et al., 1997; Matcheva and Strobel, 1999; Hickey et al., 2000; Schubert et al., 2003) or precipitation of energetic ions from the jovian magnetosphere (Waite et al., 1997), or meridional transport of energy deposited in the auroral zones (Achilleos et al., 1998), or some combination of all three processes. In any case, our understanding of these processes is insufficient to support confident predictions about the thermospheric temperature of a gas-giant planet at large orbital distances.

Despite these difficulties, it is not unreasonable to apply aeronomical models to EGPs. Several factors suggest that the ionospheres of EGPs may be more easily understood than that of Jupiter. The thermospheric temperature of EGPs should be higher than that of Jupiter. This shortens chemical time constants, reducing the importance of transport of ions through diffusion. Also, higher temperatures should help equilibrate H_2 vibrational levels and make any non-thermal distribution less important. In addition, there is reason to hope that the thermospheric temperature on an EGP can be more easily understood than on Jupiter. Although it is possible that wave heating or magnetospheric interactions dominate, it is reasonable to suppose that the primary energy source is the tremendous amount of stellar EUV radiation deposited in the EGP thermospheres. These conjectures need

to be tested through observations, but they seem sufficient to justify a first look at the aeronomy of extra-solar giant planets.

2. Model description

Calculations of the upper atmospheric structure of an EGP must be very general. In Solar-System studies one can usually assume that the major atmospheric constituent is unaffected by chemistry, but, with the large amounts of energy deposited in their atmosphere, this may not be a safe assumption for EGPs. At the outset, it is not clear if the dominant constituent is H_2 or H, created from dissociation of H_2 , or H^+ , created by photoionization of H and H_2 . Thus, chemical calculations must be capable of dealing with both neutral and ionized atmospheres and must dispense with the usual approach of calculating the chemistry of minor constituents in a background of an inert primary constituent. The calculations must treat all possible constituents in an equivalent manner. In addition, the temperature and composition of EGP thermospheres are tightly coupled through the density of the radiatively active H_3^+ molecule; thus, the thermal structure and composition must be calculated self-consistently. Coupling between temperature and composition may also occur through heating efficiencies and thermal conduction rates that depend on composition and a species-dependent escape rate. Also, chemical reaction rates and diffusion rates depend on temperature and on EGPs the range of possible temperatures is so large that it may imply widely different consequences for composition.

This investigation into the aeronomy of EGPs is based on one-dimensional (1D) models that are intended to simulate the global-average atmospheric structure. To calculate the average, all horizontal gradients and the horizontal velocities are assumed to be zero and the absorption rate of stellar EUV flux is averaged over all latitudes and local times, taking full account of the extended nature of the atmosphere. Comparison of 1D and 3D models for Titan's thermosphere provide one validation of this approach (Müller-Wodarg et al., 2000). Of course, the rotation of an EGP is likely to be tidally locked to the central star so that the star-facing hemisphere is constantly illuminated and the opposite hemisphere in constant darkness. Some of the energy deposited on the illuminated hemisphere will be transported to the dark hemisphere, but large horizontal variations may still exist. It would be interesting to explore horizontal variations, but knowledge of the basic physical balances in the atmosphere is a prerequisite for such an investigation and this knowledge is best obtained with a 1D model.

The calculations presented here encompass the regions from $1R_p$, where the pressure is 200 dyne cm^{-2} , to $3R_p$; but the calculations are most accurate from a pressure of $\sim 1 \text{ dyne cm}^{-2}$ to $\sim 2R_p$. The calculations neglect processes such as stratospheric chemistry and radiative transfer in molecular vibrational bands, that become important in Jupiter's atmosphere at pressures greater than 1 dyne cm^{-2} .

At distances of $\sim 2R_p$ from the planet, stellar gravitation and stellar radiation pressure become important and gas densities become so low that the approximations implicit in the hydrodynamic equations become questionable. In this region, full solution of the Boltzmann is probably the best approach to calculations of atmospheric structure. At the date of writing, neither chemical models for the stratosphere or kinetic models for the exosphere have been published. Eventually, it may be worthwhile to couple the thermospheric models described here to stratospheric and exospheric models in order to study the transition between regions in more detail. In the meantime, it is prudent to bear in mind that the models are most relevant for the thermosphere proper and are less accurate near the upper and lower boundary.

The results of [Goukenleuque et al. \(2000\)](#) are used as a guide to the choice of conditions at the lower boundary. Although these calculations were carried out for 51 Peg b, the basic planetary parameters are similar enough to HD209458b that the temperatures calculated by [Goukenleuque et al. \(2000\)](#) should be relevant. The [Goukenleuque et al. \(2000\)](#) calculations extend to 100 dyne cm^{-2} , and show that in this region the temperature is roughly constant and equal to the skin temperature of the planet, which is approximately 750 K. The calculations presented here have a temperature difference of less than 300 K between 200 and 1 dyne cm^{-2} . The fact that the upper boundary of the stratosphere calculation and the lower boundary of the thermosphere calculation are both roughly isothermal suggests that only small errors are introduced by not modeling the transition accurately. Moreover, the calculated temperatures in the thermosphere are tens of thousands of kelvins higher than at the lower boundary, so errors of hundreds of kelvins near the base of the atmosphere are unimportant.

2.1. Composition

The composition is calculated by solving the 1D continuity and diffusion equations in spherical geometry

$$\frac{\partial N_j}{\partial t} = P_j - L_j N_j - \frac{1}{r^2} \frac{d}{dr} r^2 \Phi_j, \quad (1)$$

where for neutrals,

$$\Phi_n = u N_n - (1 - N_n/N) D_n \left[\frac{dN_n}{dr} + N_n \left(\frac{m_i g}{k T_n} + \frac{1}{T_n} \frac{dT_n}{dr} \right) \right], \quad (2)$$

and for ions,

$$\Phi_i = u N_i - (1 - N_i/N) D_i \left[\frac{dN_i}{dr} + N_i \left(\frac{m_i g}{k T_i} + \frac{T_e/T_i}{N_e} \frac{dN_e}{dr} + \frac{1}{T_i} \frac{d(T_e + T_i)}{dr} \right) \right]. \quad (3)$$

In Eqs. (1)–(3), P_j is the production rate for the j th species, L_j the loss rate, N_j the volume number density, Φ_j the flux, D_j the diffusion coefficient, T_n the neutral temperature, g

is the acceleration of gravity, T_i the ion temperature, T_e the electron temperature, N_e is the electron density, N the total density of the atmosphere, N_n is the density of the n th neutral species, and N_i is the density of the i th ion species. The quantity u is the vertical velocity of the atmosphere, defined as the mean velocity of the different constituents, weighted by their mass density.

It is assumed that, as on Jupiter, the homopause occurs at about $\sim 1 \text{ dyne cm}^{-2}$ so that heavy constituents such as CH_4 , CO , NH_3 , and H_2O are absent from the thermosphere. This is an essential assumption because it limits the species in the upper atmosphere to compounds that can be constructed from the lightest constituents. The models include the neutral species H_2 , He , and H , and the ionized species H^+ , H_2^+ , H_3^+ , He^+ , and HeH^+ . [Table 1](#) lists the chemical reactions among these species. J -values are calculated assuming that the stellar output is similar to that of the Sun and using the November 3, 1994 solar spectrum of [Woods et al. \(1998\)](#). In addition to reactions commonly adopted in studies of jovian aeronomy, [Table 1](#) includes reactions that become important at high temperatures, such as thermal decomposition of H_2 (R4) and reaction of H^+ with vibrationally excited H_2 (R9). The rate for this latter reaction has not been measured and the value in [Table 1](#) is estimated to be the product of the collision rate and the relative population of H_2 in the $v = 4$ state ([Majeed and McConnell, 1991](#)).

Ions typically diffuse along magnetic field lines, whereas neutrals diffuse primarily in the radial direction. We have no information on the magnetic fields of EGPs and, moreover, are interested in globally-averaged models, and therefore assume that ion diffusion is also vertical. In addition, although the equations are written in their general forms, the calculations assume that $T_i = T_e = T_n = T$.

The densities of H_2 and He are held fixed at the lower boundary, where the He mole fraction is assumed to be 10%, similar to the jovian value. Other species are assumed to be in chemical equilibrium at the lower boundary. The density gradient at the upper boundary for all species is calculated by assuming that each species has an upward velocity equal to its escape velocity. Initially, both neutrals and ions are assumed to escape freely, but subsequent models address the possibility that ions are prevented from escaping by a strong magnetic field. The escape of electrons is not considered explicitly, but rather the electrons and ions are assumed to escape together. This is modeled by reducing the ion mass by a factor of two in the calculation of the escape rate.

The molecular diffusion coefficient for the i th species is calculated from

$$\frac{1}{D_i} = \sum_j \frac{N_i N_j}{N b_{ij}}, \quad (4)$$

where b_{ij} is the binary diffusion parameter. For ion–ion and ion–neutral collisions, b_{ij} is calculated from the formulae in [Banks and Kockarts \(1973\)](#). Binary diffusion parameters for neutral–neutral collisions are obtained from [Mason and Marrero \(1970\)](#).

Table 1
Chemical reactions

Reaction	Rate ^a	Reference
R1a	$\text{H}_2 + h\nu \rightarrow \text{H}_2^+ + e$	2.68×10^{-5} Yan et al. (1998)
R1b	$\rightarrow \text{H}^+ + \text{H} + e$	8.93×10^{-7} Yan et al. (1998)
R2	$\text{H} + h\nu \rightarrow \text{H}^+ + e$	4.76×10^{-5} Hummer and Seaton (1963)
R3	$\text{He} + h\nu \rightarrow \text{He}^+ + e$	2.58×10^{-5} Yan et al. (1998)
R4	$\text{H}_2 + \text{M} \rightarrow \text{H} + \text{H} + \text{M}$	$1.5 \times 10^{-9} e^{-4.8E4/T}$ Baulch et al. (1992)
R5	$\text{H} + \text{H} + \text{M} \rightarrow \text{H}_2 + \text{M}$	$8.0 \times 10^{-33} (300/T)^{0.6}$ Ham et al. (1970)
R6	$\text{H}_2^+ + \text{H}_2 \rightarrow \text{H}_3^+ + \text{H}$	2.0×10^{-9} Thread and Huntress (1974)
R7	$\text{H}_3^+ + \text{H} \rightarrow \text{H}_2^+ + \text{H}_2$	2.0×10^{-9} Estimated
R8	$\text{H}_2^+ + \text{H} \rightarrow \text{H}^+ + \text{H}_2$	6.4×10^{-10} Kapas et al. (1979)
R9	$\text{H}^+ + \text{H}_2(v \geq 4) \rightarrow \text{H}_2^+ + \text{H}$	$1.0 \times 10^{-9} e^{-2.19E4/T}$ Estimated (see text)
R10a	$\text{He}^+ + \text{H}_2 \rightarrow \text{HeH}^+ + \text{H}$	4.2×10^{-13} Schauer et al. (1989)
R10b	$\rightarrow \text{H}^+ + \text{H} + \text{He}$	8.8×10^{-14} Schauer et al. (1989)
R11	$\text{HeH}^+ + \text{H}_2 \rightarrow \text{H}_3^+ + \text{He}$	1.5×10^{-9} Bohme et al. (1980)
R12	$\text{HeH}^+ + \text{H} \rightarrow \text{H}_2^+ + \text{He}$	9.1×10^{-10} Kapas et al. (1979)
R13	$\text{H}^+ + e \rightarrow \text{H} + h\nu$	$4.0 \times 10^{-12} (300/T_e)^{0.64}$ Storey and Hummer (1995)
R14	$\text{He}^+ + e \rightarrow \text{H} + h\nu$	$4.6 \times 10^{-12} (300/T_e)^{0.64}$ Storey and Hummer (1995)
R15	$\text{H}_2^+ + e \rightarrow \text{H} + \text{H}$	$2.3 \times 10^{-8} (300/T_e)^{0.4}$ Auerbach et al. (1977)
R16a	$\text{H}_3^+ + e \rightarrow \text{H}_2 + \text{H}$	$2.9 \times 10^{-8} (300/T_e)^{0.65}$ Sundström et al. (1994)
R16b	$\rightarrow \text{H} + \text{H} + \text{H}$	$8.6 \times 10^{-8} (300/T_e)^{0.65}$ Datz et al. (1995)
R17	$\text{HeH}^+ + e \rightarrow \text{He} + \text{H}$	$1.0 \times 10^{-8} (300/T_e)^{0.6}$ Yousif and Mitchell (1989)

^a Two body rates are in $\text{cm}^3 \text{s}^{-1}$ and three body rates in $\text{cm}^6 \text{s}^{-1}$. Photolysis rates (s^{-1}) are optically thin values at 0.05 AU. The solar spectrum of Woods et al. (1998) is used to represent the stellar EUV flux.

2.2. Thermal structure

The thermal structure calculations include stellar energy deposition, thermal conduction, radiative emissions, advection, and adiabatic cooling. The temperature profile is obtained through solution of the energy balance equation

$$\rho c_p \frac{\partial T_n}{\partial t} - \frac{\partial p}{\partial t} = Q_o - Q_r + \frac{1}{r^2} \frac{d}{dr} r^2 \kappa \frac{dT_n}{dr} - u \left(\rho c_p \frac{\partial T_n}{\partial r} - \frac{\partial p}{\partial r} - \frac{p}{m} \frac{\partial m}{\partial r} \right), \quad (5)$$

where p is the pressure, ρ is the mass density, c_p is the specific heat at constant pressure, m is the mean molecular mass of the atmosphere, and κ is the thermal conduction coefficient. Q_o is the heating rate due to absorption of stellar radiation, Q_r the cooling due to radiative emissions. The third term on the RHS represents the divergence of the thermal conduction flux, and the fourth term on the RHS represents the combined effects of work done by pressure and advection and is usually referred to as adiabatic cooling.

The stellar heating rate, Q_o includes contributions from exothermic reactions and energy transfer from energetic photoelectrons to the ambient atmosphere. Chemical heating rates for the reactions in Table 1 are calculated from heats of formation and are obtained from Lias et al. (1988). The chemical heating rate is not necessarily positive because both exothermic and endothermic reactions are important. For example, thermal decomposition of H_2 (R4) is endothermic by 436 kJ mol^{-1} ; thus some of energy deposited in the atmosphere goes into dissociating H_2 rather than heating the

atmosphere. Also, the chemical heating rates are not local because chemical species, particular H, can diffuse to other locations, where subsequent reactions convert chemical energy back into heat.

Photoelectrons lose energy to the ambient atmosphere through elastic and inelastic collisions with neutrals and through Coulomb collisions with ions and thermal electrons. The energy not transferred to the ambient atmosphere is lost to the planet through excitation of UV emissions, photoelectron escape, etc. The models assumes that the extra energy acquired by the photoelectron in an ionization event is transferred to the ambient atmosphere with an efficiency of 63%. This value comes from the photoelectron transport calculation for the jovian atmosphere in Waite et al. (1983). The value of 63% is probably not accurate for an EGP and should be viewed as a rough guess, but it is unlikely to be incorrect by more than tens of percent. More accurate estimates could be obtained with a photoelectron transport calculation, but the approach adopted here is sufficient for this first investigation of EGP aeronomy.

The important radiative emissions include IR radiation from H_3^+ and radiation from H^+ recombination. The H_3^+ cooling rate is taken from Neale et al. (1996) and the H^+ recombination cooling rate from Seaton (1960). The cooling rate is calculated by assuming optically thin emissions and neglecting absorption of radiation from the lower atmosphere. The results show that these approximations are accurate because optical depths are low and calculated atmospheric temperatures greatly exceed those in the lower atmosphere.

The thermal conduction flux can be carried either by neutrals, ions, or electrons. On Jupiter, the thermal conduction flux is carried primarily by neutrals, because the electron density is low. This may not be the case if an EGP has a robust ionosphere and neutral, electron, and ion conductivity must be allowed for. The electron conductivity is calculated from

$$\kappa_e = \frac{\kappa_{ei}}{1 + \kappa_{ei} \sum_k (1/\kappa_{en})}, \quad (6)$$

where the κ_{ie} term, due to electron–ion collisions, is given by

$$\kappa_{ei} = 1.2 \times 10^{-6} T_e^{5/2} \text{ erg cm}^{-1} \text{ s}^{-1} \text{ K}^{-1}, \quad (7)$$

and the κ_{en} term, due to electron–neutral collisions, is given by

$$\kappa_{en} = 1.2 \times 10^{-6} \frac{N_e}{N_n} T_e^{1/2} \text{ erg cm}^{-1} \text{ s}^{-1} \text{ K}^{-1}. \quad (8)$$

The ion conductivity is given by

$$\kappa_i = \frac{7.4 \times 10^{-8}}{\sqrt{\mu}} T_i^{5/2} \text{ erg cm}^{-1} \text{ s}^{-1} \text{ K}^{-1}, \quad (9)$$

where μ is the reduced mass for the ion–neutral collision. All of these expressions are obtained from [Banks and Kockarts \(1973\)](#). The neutral conductivity is calculated from

$$\kappa_n = \sum_j \frac{\kappa_j N_j}{r} \sum_k N_k \phi_k, \quad (10)$$

κ_j is the thermal conductivity of the j th constituent and ϕ_k is given by

$$\phi_k = \frac{(1 + (\mu_i/\mu_j)^{1/2} (m_j/m_i)^{1/4})^2}{2\sqrt{2} (1 + (m_i/m_j))^{1/2}}, \quad (11)$$

where μ_i is the viscosity of the i th constituent ([Banks and Kockarts, 1973](#)).

2.3. Momentum balance

The vertical momentum equation is

$$\frac{\partial u}{\partial t} = -u \frac{\partial u}{\partial r} - \frac{1}{\rho} \frac{\partial p}{\partial r} - g + \frac{1}{\rho} \frac{1}{r^2} \frac{\partial}{\partial r} \left(r^2 2\mu \frac{\partial u}{\partial r} \right) - \frac{4\mu u}{\rho r^2}, \quad (12)$$

where the first term on the RHS represents advection, the second term is the pressure gradient, the third term gravity, and the fourth and fifth, viscous deceleration of the gas. The quantity μ is the coefficient of viscosity.

After using the equation of state to related density and pressure, [Eq. \(12\)](#) can be integrated to give the pressure in terms of gravity and the bulk velocity in steady-state

$$p(r) = p_o \exp \left(- \int \frac{GM}{R_g T} \frac{dr}{r^2} - \int \frac{\partial u^2}{\partial r} \frac{dr}{2R_g T} + \int \left(\frac{2}{R_g T} \frac{\partial}{\partial r} \left(r^2 \mu \frac{\partial u}{\partial r} \right) - \frac{4\mu u}{R_g T} \right) \frac{dr}{r^2} \right), \quad (13)$$

where R_g is the gas constant. The first factor on the RHS of [Eq. \(12\)](#) represents the usual barometric variation of pressure, the second factor represents the effects of advection, and the third factor represents the effects of viscosity. The velocity can be obtained from the mass continuity equation and the mass density through

$$\rho u r^2 = \text{constant}. \quad (14)$$

The constant in this expression comes from the velocity at the upper boundary, which is set equal to the weighted average of the escape velocity of the individual constituents. [Equations \(13\)](#), [\(14\)](#), and the ideal gas law are then solved iteratively for consistent solutions of p , u , and ρ .

2.4. Escape

The escape rate of the EGP atmosphere is enhanced by the upward bulk velocity at the top of the atmosphere. This situation is analogous to the solar wind and is often referred to as “blow off” ([Hunten, 1982](#)) and has previously been examined for models of the early Earth and Venus ([Kasting and Pollack, 1983](#)) and for Pluto ([McNutt, 1989](#); [Hubbard et al., 1990](#); [Krasnopolsky, 1999](#)). These earlier calculations, following the approach taken in studies of the solar wind, ensured supersonic solutions to the momentum equation by requiring zero pressure at infinite distances from the planet. A different approach is followed here because, as mentioned previously, the effects of stellar gravity and the interaction of the escaping atmosphere with the stellar wind are important at distances of several planetary radii. Thus, extending the calculation to infinity is questionable, even for the purposes of calculating the escape rate.

The alternative to extending the calculations beyond their region of validity is to apply boundary conditions at a closer distance where the 1D hydrodynamic equations are more nearly valid. The distance of $3R_p$ is chosen as a reasonable compromise that encompasses most of the aeronomical processes of interest while the effects of stellar gravity are still minor. The boundary conditions are derived from the requirement of consistency between the hydrodynamic description of the gas flow and the kinetic description. That is, the mean outflow velocity implied by the molecular velocity distribution functions is required to be equal to the bulk velocity of the atmosphere,

$$\rho u = \pi \sum_i m_i \int_{v_{\text{esc}}}^{\infty} v^3 f_i(\vec{v}) dv, \quad (15)$$

where the sum is over the molecular species in the atmosphere, m_i is the molecular mass of the i th species, v is the molecular velocity, and v_{esc} is the escape velocity. The molecular velocity distribution function $f_i(\vec{v})$ is assumed to be a convected Maxwellian in order to be consistent with the degree of approximation used to derive the Navier–Stokes equations from the Boltzmann equation ([Chapman and Cowling, 1970](#)).

If the bulk velocity of the atmosphere were very small the approach described above would yield the conventional expression for the Jeans escape rate. The approach is also capable of treating supersonic outflow at the upper boundary, though this does not occur in the cases considered here. However, upward velocities large enough to dominate the thermal structure of the atmosphere are obtained, so the escape of the atmosphere is in the blow-off regime, as defined by [Hunten \(1982\)](#).

2.5. Numerical method

The coupled momentum, energy, and continuity equations are solved by integrating to a steady state. The continuity equation is the first to be solved in each time step utilizing values for velocity and temperature from the previous time step. The energy equation is solved next, using the updated values for densities. The momentum equation is the last to be solved in each time step iteration, using the updated values for densities and temperature. The continuity equations for the individual species and the energy equation are solved using a fully implicit technique to advance to the next time step. As discussed above, the vertical momentum and mass continuity equations are solved together in iterative fashion, to find a steady state solution at each time step. The calculations are carried out on an altitude grid with equal spacing in $1/r$, which is a more natural coordinate for extended atmospheres than altitude itself. The atmosphere is divided into 300 layers from $1R_p$, where the pressure is set to 200 dyne cm^{-2} , to $3R_p$. The pressure at the upper boundary depends on the temperature profile, and varies from 10^{-5} to $5 \times 10^{-4} \text{ dyne cm}^{-2}$ for the range of models considered here. A time step of 1000 s is used to integrate to steady state. Calculations are run until all equations balance to better than 0.1% in all atmospheric layers.

3. Results

A reference model is described first in order to focus the discussion and facilitate an in-depth examination of the relevant physical balances prevailing in the atmosphere. The reference model used here adopts parameters similar to those of HD209458b, specifically a mass of $0.6M_J$, a radius at 200 dyne cm^{-2} equal to $1.4R_J$ and a star-planet distance of 0.05 AU. After discussion of the reference model, trends with changes in semi-major axes are considered in order to examine the range of plausible conditions in an EGP atmosphere and to investigate the sensitivity of atmospheric structure to the stellar EUV flux.

3.1. Reference model

[Figure 1](#) shows a summary of results for the reference model. The thermospheric temperature rises to values greater than 12,000 K. This causes a greatly extended

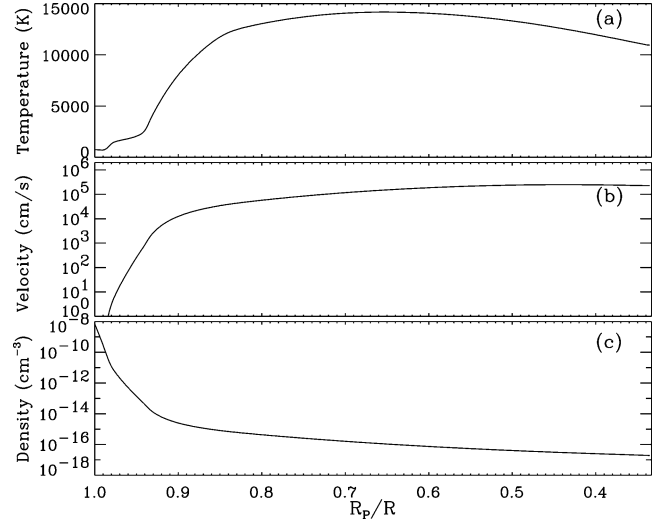


Fig. 1. The altitude distributions of (a) temperature, (b) velocity, and (c) mass density for the reference model.

atmosphere with significant density to beyond $3R_p$. The extent of the atmosphere is determined primarily by the λ parameter defined by

$$\lambda = \frac{GMm}{kTr}. \quad (16)$$

At the base of the atmosphere $\lambda = 313$, which is fairly close to the jovian value of 474. However, at $3R_p$, λ has decreased to 5.6, as a result of the high temperatures and lower gravity. The barometric pressure in an extended isothermal atmosphere in hydrostatic equilibrium varies as

$$p = p_0 e^{\lambda - \lambda_0}. \quad (17)$$

For small values of λ the decrease of pressure and density with distance is gradual, as shown in [Fig. 1c](#). In fact, a value of $\lambda_0 = 5.6$ at a pressure of $10^{-5} \text{ dyne cm}^{-2}$ implies a pressure of $3.7 \times 10^{-8} \text{ dyne cm}^{-2}$ at $\lambda = 0$ or $r = \infty$. This is much greater than the pressure in interplanetary space, implying that the atmosphere cannot be hydrostatic, but must be escaping in a manner similar to that of the solar wind. It is this fact that requires that the full vertical momentum equation be solved, rather than the usual hydrostatic approximation. The upward velocity of the atmosphere, shown in [Fig. 1b](#), plays a critical role in the structure of EGP thermospheres and is one of the primary differences between the jovian upper atmosphere and an EGP upper atmosphere.

The composition of the atmosphere is shown in [Fig. 2](#) and the important chemical reactions for the reference model are shown in [Fig. 3](#). Although the main species at the lower boundary are H_2 and He, the lower thermosphere is primarily H and the upper thermosphere H^+ . H_2 is quickly converted to H by thermal decomposition (R4). This process becomes important once the temperature reaches $\sim 2000 \text{ K}$. Photoionization makes only a minor contribution to the destruction of H_2 . The column-integrated H_2 destruction rate due to R4 is $4.0 \times 10^{12} \text{ cm}^{-2} \text{ s}^{-1}$, compared with $9.5 \times$

$10^{11} \text{ cm}^{-2} \text{ s}^{-1}$ for R1. The transition from H_2 to H strongly affects the atmosphere because the mean molecular mass drops by a factor of two and the scale height doubles. Helium also quickly disappears with increasing altitude because of diffusive separation. At higher altitudes, H^+ becomes the dominant species, created by photoionization of H . The density of H^+ is regulated by an approximate balance between photoionization (R2) and advection. Loss of H or H^+ by diffusion is minor, partly because of the large scale heights in the atmosphere.

The calculated H_3^+ densities are relatively low. This is due to the rapid loss of H_2 and the resulting decrease in H_2 photoionization rates and to the short lifetime of H_3^+ , which is related to the large electron density, associated with the high H^+ density. It is interesting that photoionization creates both H_2^+ , which is quickly converted to H_3^+ and H^+ and its associated electrons, which cause the destruction of H_3^+ . This

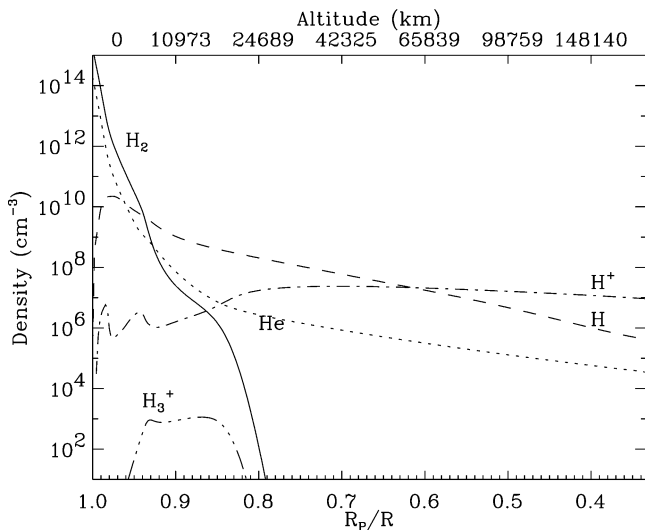


Fig. 2. The composition of the reference model.

leads to the somewhat surprising situation that an increase in the photoionization rate can cause a decrease in the H_3^+ density. The calculated H_3^+ density for the reference model is smaller than that in Jupiter's ionosphere, typically calculated to be 10^4 – 10^5 cm^{-3} (Majeed and McConnell, 1991). Despite its low density, it is shown below that H_3^+ plays a critical role in the thermal structure.

The important terms in the energy balance equation are shown in Fig. 4. Stellar heating in the upper thermosphere is balanced primarily by adiabatic cooling. Cooling due to radiation and to the divergence of the thermal conduction flux is not significant. This differs from most planetary thermospheres where energy is carried away primarily by thermal conduction. The adiabatic cooling is a result of rapid atmospheric escape and is responsible for the gradual decrease in temperature with increasing distance above $R_p/R = 0.7$. Lower in the thermosphere, stellar energy deposition is balanced primarily by H_3^+ cooling. This is surprising considering the low H_3^+ densities, but H_3^+ is an effective coolant at high temperature (Neale et al., 1996). The weakness of thermal conduction is due to the large scale heights in the atmosphere. The rate of cooling due to thermal conduction varies roughly as κ/H_o^2 , where H_o is the scale height of the atmosphere; thus thermal conduction becomes less important as H_o becomes large.

Figure 4 also shows the heating efficiency, defined as the ratio of the net heating rate to the rate of stellar energy absorption. Low in the thermosphere, where the composition is primarily H_2 , the heating efficiency is 50–60%, consistent with that for the jovian atmosphere (Waite et al., 1983). Higher in the thermosphere, the heating efficiency drops to $\sim 10\%$. This low value obtains because much of the absorbed stellar energy goes into ionizing H . This energy is either lost through escape of H^+ or, upon recombination of H^+ , the chemical energy is converted to radiant energy, i.e., a photon, that escapes the atmosphere. As a conse-

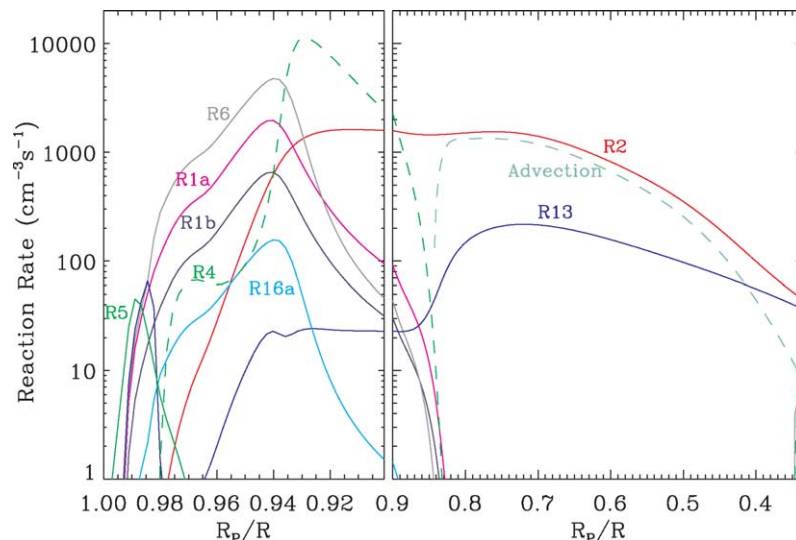


Fig. 3. The primary chemical reaction rates in the reference model. Reaction R16b is not shown but is nearly equal to R6.

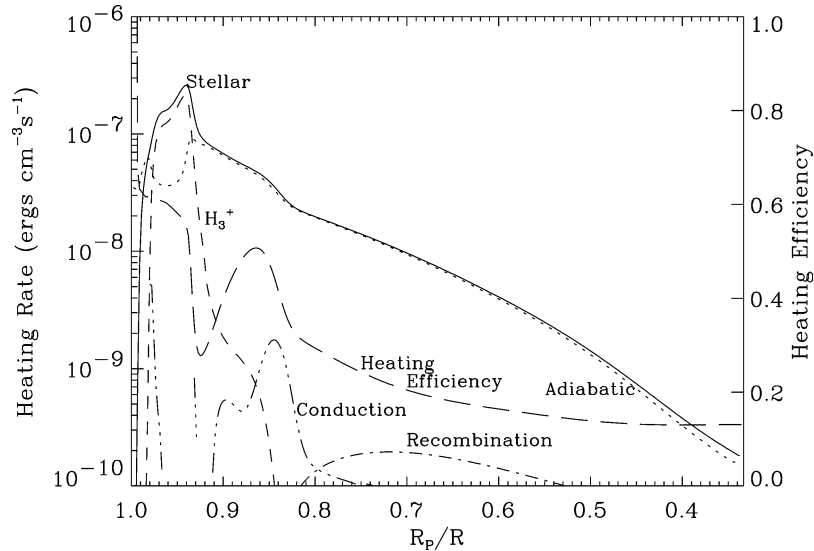


Fig. 4. Heating rates and heating efficiencies in the reference model. The solid line represents the net heating rate in the atmosphere. Other terms represent cooling rates by the processes indicated.

quence, most stellar EUV energy absorbed by H escapes the atmosphere and does not contribute to local heating. This differs from recombination of H_2^+ or H_3^+ lower in the thermosphere, which returns chemical energy to the atmosphere through the kinetic energy of the reactant products.

Solution of the momentum equation reveals that the atmosphere is close to hydrostatic balance, despite the large escape rate. Figure 5 shows that gravitational acceleration is balanced primarily by the pressure gradient. Advection of momentum is minor, with a contribution less than 5% at all levels. Viscous forces are negligible. The dominance of hydrostatic balance is consistent with the fact that the velocity of the atmosphere, though large, is sub-sonic. The speed of sound at 12,000 K is roughly 10 km s^{-1} , whereas the atmospheric velocity has a value at $3R_P$ of 2.4 km s^{-1} . Thus, the velocity is large enough to have dominant effect on the temperature profile, but still has a minor effect on the density profile. Or, more accurately, the primary way that the velocity influences the density is through modification of the temperature profile rather than through modification of hydrostatic balance. Presumably, the planetary wind becomes supersonic at greater distances from the planet, but that region is not modeled here.

The momentum and energy balance in the atmosphere are coupled through the adiabatic cooling term. The dominance of the adiabatic cooling term in the upper thermosphere indicates that much of the stellar energy deposited in the atmosphere goes into lifting the atmosphere. Examination of the column-integrated rates confirm this conclusion. The column-integrated rates for stellar heating, H_3^+ cooling, and adiabatic cooling are 351 , 81 , and $267 \text{ erg cm}^{-2} \text{ s}^{-1}$, respectively, with radiative recombination and thermal conduction making up the small remainder. The adiabatic heating rate represents the energy required to raise thermospheric gases in the presence of a gravitational field. This term is zero in

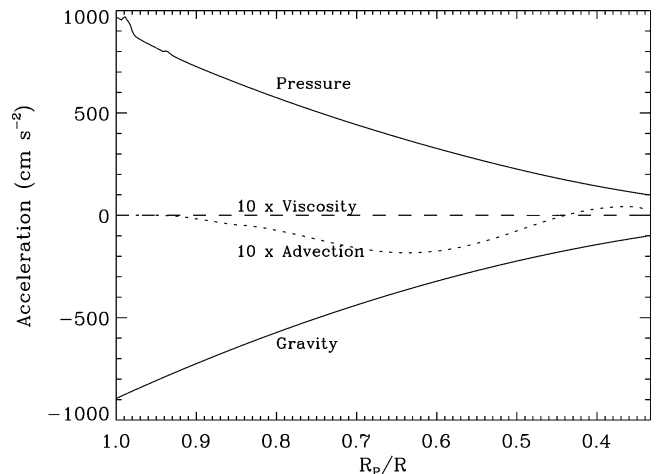


Fig. 5. Accelerations in the reference model.

a static atmosphere and is therefore a direct consequence of rapid atmospheric escape. Thus, the energy balance indicates that most of the stellar energy deposited in the atmosphere goes into powering escape. This conclusion is supported by the variation of escape rate with stellar insolation, presented in Section 3.3 below.

3.2. Inhibited ion escape

While neutrals are free to escape at the kinetic rate, ions may be inhibited from doing so by a planetary magnetic field. Presently, there is no evidence for or against an intrinsic magnetic field on EGPs, but, based on analogy with the jovian planets, a strong field is a possibility. A magnetic field will inhibit ion escape as long as the magnetic pressure is greater than the plasma pressure. Because the flow is sub-sonic, the plasma pressure is due primarily to its thermal energy and the magnetic pressure is greater than the plasma

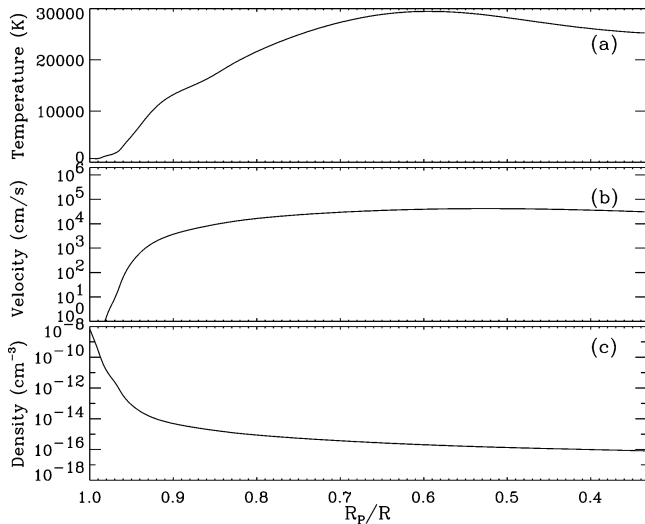


Fig. 6. The same as Fig. 1 but for a model with ion escape inhibited.

pressure if

$$\frac{B^2}{8\pi} > N_i k T_i + N_e k T_e. \quad (18)$$

The plasma pressure at the upper boundary of the reference model is 3.4×10^{-5} dyne cm^{-2} . If an EGP has an intrinsic magnetic field strength at $1R_P$ of 4.3 gauss (the jovian value), then the magnetic pressure is 0.74 dyne cm^{-2} , more than sufficient to confine the plasma. If the plasma pressure were constant with radial distance, the plasma and magnetic pressures would balance at $37R_P$. Of course, at sufficiently high magnetic latitudes, the B field lines of an EGP should be open to the stellar wind, allowing ions to escape by flowing along the field lines. Where this occurs depends on the interaction between the stellar wind and the EGP magnetosphere and, based on experience with the planets in our Solar System, this is likely to be a complex interaction. Full investigation of this area is outside the scope of this paper, but some insight into the potential effects of a magnetic field can be gained by considering the simple situation where neutrals escape at the kinetic rate, but ions are inhibited from escaping.

The results from such a model are shown in Fig. 6. Inhibiting ion escape reduces the bulk velocity of the atmosphere from 2.4 km s^{-1} at $3R_P$ in the reference model to 0.4 km s^{-1} in the model with inhibited ion escape. The lower velocity reduces the amount of adiabatic cooling leading to temperatures about 10,000 K higher in the inhibited ion escape model than the reference model. As a consequence, the densities at high altitudes are roughly a factor of 5 larger in the model with inhibited ion escape than in the reference model. However, the net escape rate with ion escape inhibited is only $\sim 30\%$ smaller than in the reference model, because the higher temperatures and densities cause an increase in the H escape rate that compensates for the decrease in the H^+ escape rate.

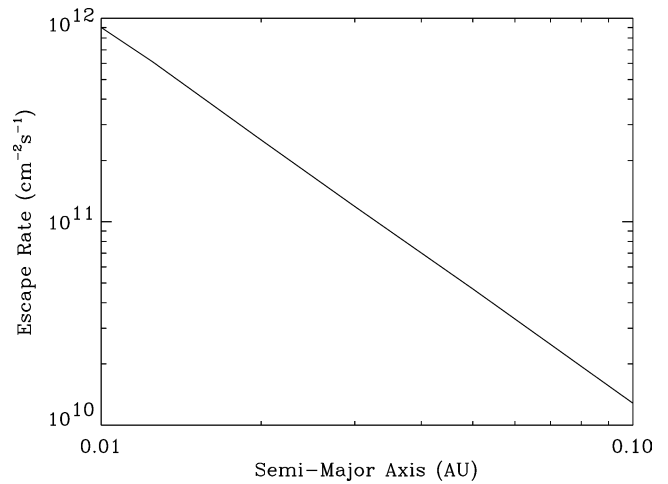


Fig. 7. Escape rate versus semi-major axis.

3.3. Trends with semi-major axis

The nature of atmospheric escape from an EGP can be explored further through examination of trends with semi-major axis. Figure 7 shows the calculated escape rate as a function of distance from the central star for an assumed circular orbit. The calculations assume that both neutrals and ions escape at the kinetic rate. The ratio of escape rates for $a = 0.01$ and $a = 0.05$ AU is a factor of 20, only 20% less than the ratio of incident stellar flux, thus the escape rate varies roughly as the stellar flux. This indicates that the escape rate is energy limited, i.e., the escape flux is not determined by the temperature of the atmosphere, but by the amount of stellar EUV energy absorbed in the upper atmosphere. The existence of an energy limit to the escape rate was first postulated by Watson et al. (1981) and the concept was subsequently applied to models of the early atmosphere of Venus (Kasting and Pollack, 1983) and to models of Pluto's atmosphere (Hunten and Watson, 1982; McNutt, 1989; Hubbard et al., 1990; Krasnopolsky, 1999). The interesting point here is that the energy limit also applies for a milder wind, that is only a fraction of the speed of sound.

Figures 8 and 9 show the composition for models calculated with $a = 0.01$ and 0.1 AU. As expected, higher insolation increases the abundance of H^+ relative to H and pushes the H_2 -H transitions to lower altitudes. The H_3^+ densities are about a factor of ten larger in the $a = 0.01$ AU model than in the $a = 0.1$ AU model, varying approximately as the square root of the ionization rate. Figure 10 shows the temperature profiles for a variety of semi-major axes from 0.01 to 0.1 AU. The maximum temperatures increase by only a factor of ~ 2 for the factor of 100 variation in the stellar heating rate. This is because the increase in adiabatic cooling associated with the larger escape rates offsets the larger heating rate for the close-in models. The increased importance of adiabatic cooling can be seen in the stronger negative temperature gradient at high altitudes in the $a = 0.01$ AU model.

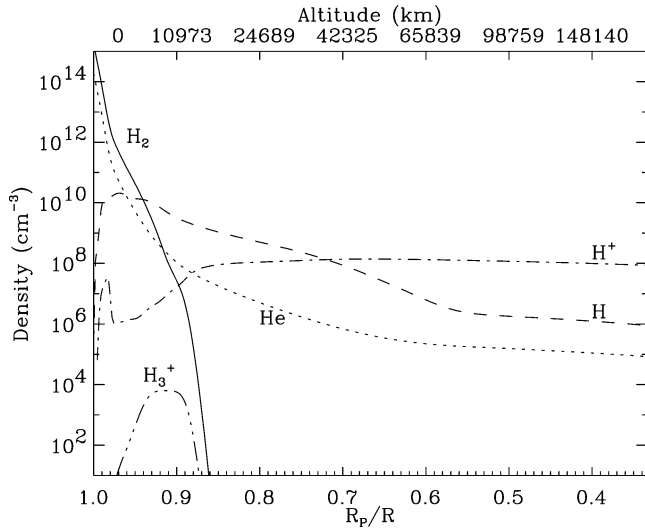


Fig. 8. Predicted composition for a semi-major axis of 0.01 AU.

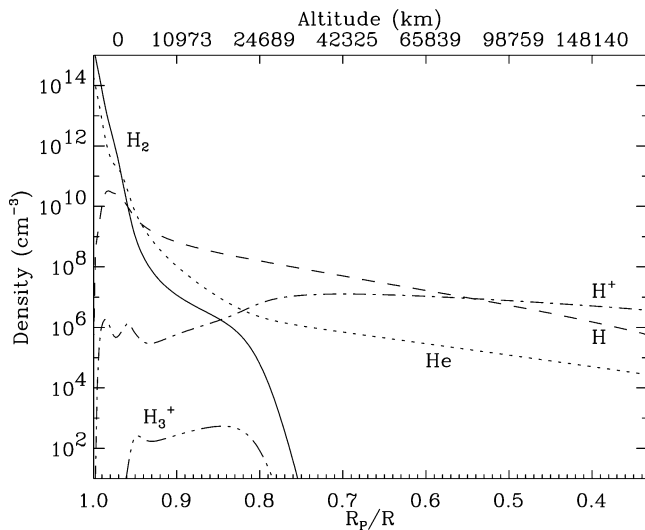


Fig. 9. Predicted composition for a semi-major axis of 0.1 AU.

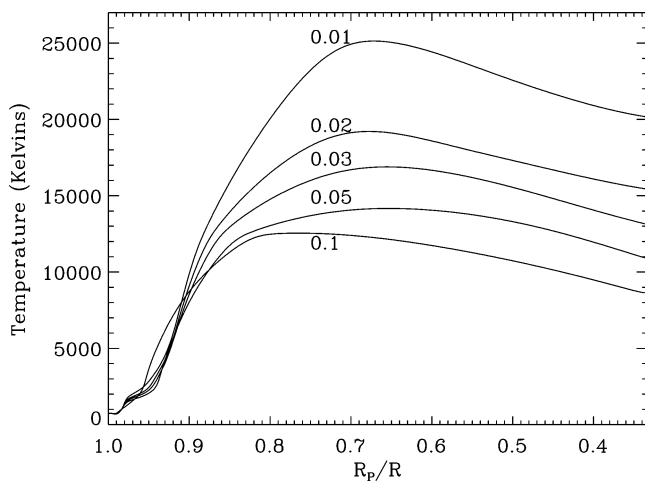


Fig. 10. Temperature profiles for a variety of planet-star distances. Semi-major axes in AU are indicated on the figure.

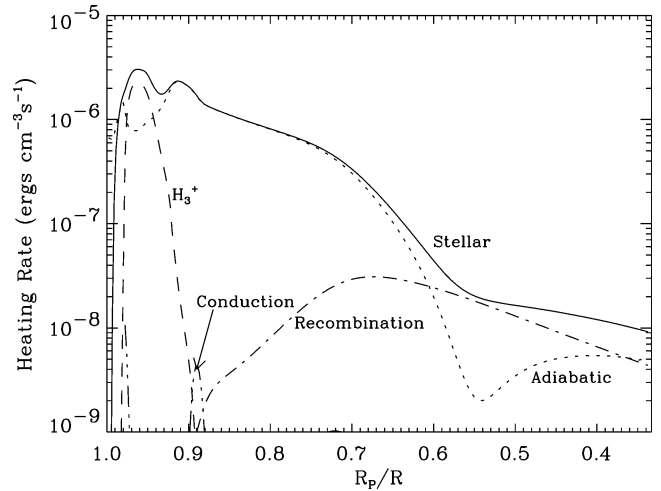


Fig. 11. The same as Fig. 4 but for the $a = 0.01$ AU model.

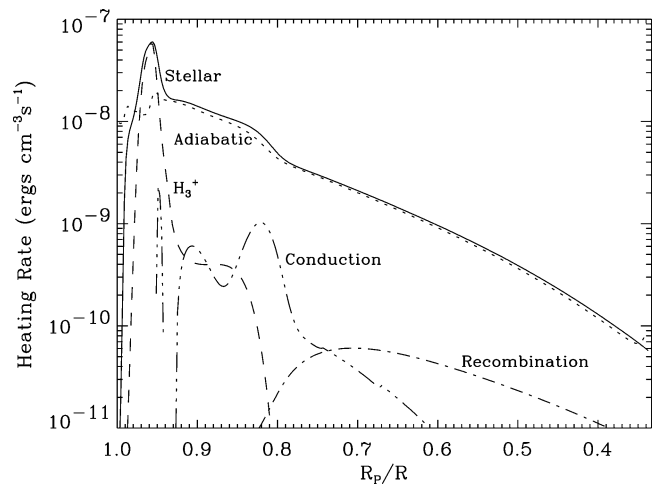


Fig. 12. The same as Fig. 4 but for the $a = 0.1$ AU model.

Figures 11 and 12 show the energy balance for the $a = 0.01$ and 0.1 AU models. The primary difference between the $a = 0.01$ AU model and the reference model is the importance of recombination cooling in the $a = 0.01$ AU model. This is counter intuitive because one would expect the larger escape rate in the $a = 0.01$ AU case to lead to stronger adiabatic cooling. However, at smaller star-planet distances the ionization fraction is larger because of the increase in ionization rate, implying an increase in the recombination rate. This effect dominates over the increase in adiabatic cooling, making recombination and adiabatic cooling of comparable importance at $3R_p$ and making recombination cooling the dominant term near $2R_p$. As with the reference model, H_3^+ cooling dominates from 1 to $1.1R_p$ in the $a = 0.01$ AU model and thermal conduction is of minor importance at all altitudes.

Based on the discussion in the previous paragraph one would expect adiabatic cooling to dominate over recombination cooling in the $a = 0.1$ AU model and Fig. 12 shows that this is in fact the case. Recombination cooling is of mar-

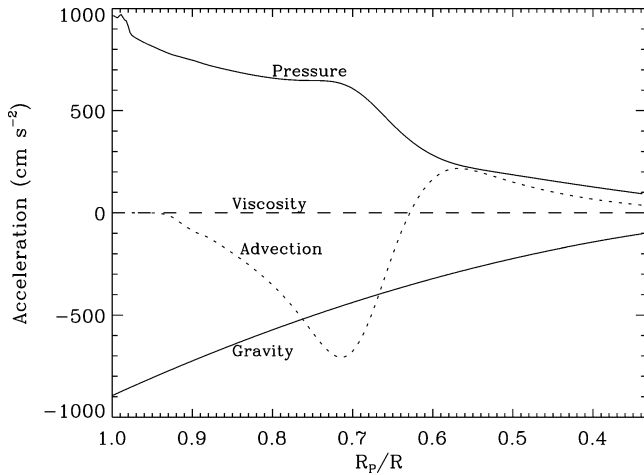


Fig. 13. The same as Fig. 5 but for the $a = 0.01$ AU model.

ginal importance in this model. Thermal conduction is relatively more important in the $a = 0.1$ AU model, contributing roughly 10% of the net cooling from 1.07 to $1.25R_p$.

Figure 13 shows the momentum balance for the $a = 0.01$ AU model. The larger velocity of the atmosphere causes vertical advection to become an important term in the momentum balance equation and the atmosphere is no longer close to hydrostatic equilibrium. Momentum balance for $a = 0.1$ AU is not shown because both viscosity and advection are negligible and the atmosphere is in hydrostatic balance to high precision.

4. Discussion

Upper atmospheric structure and escape rates for close in EGPs have also been considered by Liang et al. (2003) and Lammer et al. (2003). Liang et al. (2003) consider the chemistry of an EGP upper atmosphere, but not the thermal profile. Instead, they adopt the thermal profile of Seager et al. (2000). The Seager et al. (2000) models do not include heating by solar EUV and are therefore not appropriate for the thermosphere. In fact, the temperature profile calculated by Seager et al. decreases monotonically with altitude and temperatures are less than 1000 K at all levels in the upper atmosphere. Because the temperatures adopted by Liang et al. (2003) are low, thermal decomposition of H_2 , which is the primary source of atomic hydrogen, is not considered. Liang et al. (2003) do consider production of H by photolysis of CH_4 and H_2O and obtain a mixing ratio of several percent, indicating that much of the H bound in CH_4 and H_2O is freed by photolysis. However, because the abundance of H_2O and CH_4 is more than an order of magnitude less than H_2 , photolysis of these molecules is not a significant source of H in an EGP thermosphere. The processes considered by Liang et al. (2003) likely are the dominate source of H in the stratosphere of a close-in EGP.

The paper by Lammer et al. (2003) presents analytic approximations to the upper atmospheric temperature and es-

cape rate of close-in EGPs. Chemistry is not considered by these authors and the models appear to be for an atmosphere of constant chemical composition, though this is not explicitly mentioned in the paper. It is stated that the models do not include H_3^+ and it seems clear that they do not include H^+ either. The escape rates estimated by Lammer et al. (2003) are a factor of 20 larger than calculated here. The difference can be traced to the neglect of chemistry in the Lammer et al. models. H_3^+ damps the escape rate by cooling the base of the thermosphere while conversion of the atmosphere to H^+ at high altitudes damps the escape rate by lowering the solar energy deposition rate. Lammer et al. (2003) neglect both of these ions are therefore overestimate the escape rate. The disagreement in estimated escape rate may also be partly due to the differences between the analytic approximation employed by Lammer et al. (2003) and the rigorous solution of the vertical momentum equation presented here.

There is a qualitative agreement between the hot thermospheres calculated here and the $H Ly\alpha$ absorption measurements of Vidal-Madjar et al. (2003). The observed absorption signature has a magnitude of $\sim 15\%$. In the visible, the planet occults about 1% of the star light, so an absorption of 15% implies that H is optically thick to about $4R_p$. The reference model has an H density of $4.1 \times 10^5 \text{ cm}^{-3}$ at $3R_p$ and a temperature of 10,909 K, implying a tangential column abundance of $1.7 \times 10^{16} \text{ cm}^{-2}$. Assuming a Maxwell-Boltzmann distribution for the H cloud and using the temperature quoted above implies an absorption cross section at $Ly\alpha$ line center of $5.6 \times 10^{-14} \text{ cm}^2$ and an optical depth of ~ 1000 . Thus, the H distribution calculated here is opaque out to several planetary radii, in rough agreement with the measurements. Vidal-Madjar et al. (2003) also show that the absorption extends roughly 0.5 \AA from the center of the $Ly\alpha$ line. This only occurs if the H distribution is characterized by a high temperature. Assuming a Maxwell-Boltzmann distribution and a temperature of 10,000 K implies a Doppler broadened absorption line with a width of 0.055 \AA . An optical depth at line center of 1000 implies that optical depth unity is reached roughly 3 Doppler widths from line center or at 0.16 \AA . This is of the same order but somewhat smaller than measured by Vidal-Madjar et al. (2003).

A more quantitative comparison requires improvements to the models. As mentioned earlier, the assumptions contained in these aeronomical models become questionable at a distance of $3R_p$ from the planet. The gravitation field of the central star and radiation pressure can no longer be neglected and a 1D calculation is no longer possible. Instead it is preferable to construct kinetic models that calculate the H distribution by integrating along trajectories in the exosphere.

The calculations presented here assume that the vertical mixing rate is so low that diffusive separation ensures that there are no detectable heavy species (C, N, O, etc.) in the upper atmosphere. This is true if the vertical mixing is comparable to that in Jupiter's atmosphere, but vertical mixing

rates are impossible to predict from first principles and other assumptions are possible.

The Vidal-Madjar et al. (2003) observations demonstrate the utility of investigating the atmospheres of EGPs through the H Ly α absorption technique. It is also worthwhile to consider if there are other diagnostic spectral features that could be used to study the upper atmosphere of an EGP. The upper atmosphere of Jupiter has been investigated through analysis of emissions in the UV and near IR. Jovian H $_3^+$ emissions in the near IR have been a particularly useful probe of upper atmospheric temperatures and ion densities. H $_3^+$ is absent in stellar atmospheres and any detected emissions could safely be assumed to originate from an EGP. The H $_3^+$ distribution in an EGP thermosphere is probably best studied with the “occultation spectroscopy,” technique discussed by Richardson et al. (2003). Essentially, this consists of comparing the flux measured from the star-planet system with the EGP in front of and behind the central star. The advantages of H $_3^+$ are that the emissions are characterized by a high temperature, occur in a wavelength regions where the star is relatively dim, and extend a significant distance above the nominal radius of the EGP, the criteria mentioned by Richardson et al. (2003) as defining good candidate emissions for occultation spectroscopy. A mitigating factor is that the H $_3^+$ density is low and the emissions are optically thin. The reference model predicts an H $_3^+$ emission rate of 82 erg cm $^{-2}$ s $^{-1}$. For HD209458b at a distance of 47 pc and a radius of 1.4R $_J$, this implies a flux at the Earth of 9.7 \times 10 $^{-20}$ ergs cm $^{-2}$ s $^{-1}$. Detailed simulations are needed to determine if emissions at this level could be detected with occultation spectroscopy.

An EGP should also be bright in Lyman and Werner band emissions and again these emissions have the advantage that they do not occur in the stellar spectrum. The jovian upper atmosphere has been studied through analysis of UV emissions in the H $_2$ Lyman and Werner electronic band systems, as well as H Ly α and H $_3^+$ emissions. Adopting a wavelength-integrated disc brightness of 2 kR for the jovian emission and scaling by the planet-star distance implies a brightness of 2 \times 10 4 kR and a flux at Earth of \sim 10 $^{-8}$ photons cm $^{-2}$ s $^{-1}$ for HD209458b, assuming that emissions come from half the visible hemisphere of the EGP.

The H $_2$ Lyman and Werner band emissions could be larger than implied by scaling the jovian emission rate. For example, auroral emissions may exist in addition to dayglow emissions. On Jupiter, the auroral emissions in the H $_2$ Lyman and Werner bands are brighter than the disc-integrated emission (Yelle and Miller, 2004). In addition, fluorescent excitation of the Lyman band emissions from an EGP atmosphere may be more efficient than on Jupiter. Most of the Lyman and Werner band fluorescence from Jupiter’s thermosphere occurs from the ground vibrational state of H $_2$ because the relatively cool temperatures imply low populations of vibrationally excited molecules. The higher temperatures in an EGP atmosphere imply a higher level of vibrational excitation. This is important because it becomes

possible to absorb H Ly α radiation in the P(5) and R(6) lines of the Lyman (1, 2) band. H Ly α is by far the brightest line in the FUV spectrum of solar-type stars and absorption of this line implies much higher fluorescent intensities than would otherwise obtain. Elevated H $_2$ Lyman band emissions due to H Ly α fluorescence was observed on Jupiter after the Shoemaker–Levy 9 collisions, which caused an elevation in the temperatures of the jovian thermosphere (Wolven et al., 1997). A possible advantage to the study of Lyman and Werner band emission is that the stellar background at FUV wavelengths is relatively low. More detailed examination of the H $_2$ Lyman and Werner band emissions from EGP atmosphere will be presented in a future publication.

The results reported here are also of interest to investigations of the evolution of EGPs. Vidal-Madjar et al. (2003) have suggested that the escape rate from an EGP may be large enough to affect the evolution of the planet. The calculations presented here do not support this conclusion. The escape rate for the reference model is \sim 5 \times 10 10 cm $^{-2}$ s $^{-1}$, about 100 times smaller than inferred by Vidal-Madjar et al. (2003), and corresponds to a mass loss rate of 10 5 kg s $^{-1}$. This implies that only 3 \times 10 $^{-6}$ of the mass of the planet is lost in 1 Gyr. A mass loss rate this low should have an insignificant effect on the evolution of the planet. The Vidal-Madjar et al. value is derived from the observed H Ly α absorption signature, rather than from escape calculations but few details on the derivation are given in Vidal-Madjar et al.’s brief report and further investigation is required to determine if in fact the two results are inconsistent.

Acknowledgments

This research has been supported by grants NAG5-12699 to the University of Arizona. The author thanks Dr. J. Moses for advice on reaction rates and Drs. L. Young, C. Griffith, J. Harrington, D. Hunten, W. Hubbard, and J. Lunine for helpful discussions.

References

- Achilleos, N., Miller, S., Tennyson, J., Aylward, A.D., Mueller-Wodarg, I., Rees, D., 1998. JIM: a time-dependent, three-dimensional model of Jupiter’s thermosphere and ionosphere. *J. Geophys. Res.* 103, 20089–20112.
- Auerbach, D., Cacek, R., Candano, R., Gaily, T.D., Keyser, C.J., McGowan, J.W., Mul, P.M., Wilk, S.F.J., 1977. Merged electron–ion beam experiments. I. Method and measurements of e + H $_2^+$ and e + Hg $_3^+$ dissociative-recombination cross sections. *J. Phys. B At. Mol. Phys.* 10, 3797–3820.
- Banks, P.M., Kockarts, G., 1973. *Aeronomy*, Part B. Academic Press, San Diego.
- Baulch, D.L., Cobos, C.J., Cox, R.A., Esser, C., Frank, P., Just, T., Kerr, J.A., Pilling, M.J., Troe, J., Walker, R.W., Warnatz, J., 1992. Evaluated kinetic data for combustion modelling. *J. Phys. Chem. Ref. Data* 21, 411–744.
- Bohme, D.K., Mackay, G.I., Schiff, H.I., 1980. Determination of proton affinities from the kinetics of proton transfer reactions. VII. The proton affinities of O $_2$, H $_2$, Kr, O, N $_2$, Xe, CO $_2$, CH $_4$, N $_2$ O, and CO. *J. Chem. Phys.* 73, 4976–4986.

- Burrows, A., Lunine, J.I., 1995. Extra-solar planets—astronomical questions of origin and survival. *Nature* 378, 333.
- Chapman, S., Cowling, T.G., 1970. *The Mathematical Theory of Non-uniform Gases*. Cambridge Univ. Press, Cambridge.
- Charbonneau, D., Brown, T.M., Latham, D.W., Mayor, M., 2000. Detection of planetary transits across a Sun-like star. *Astrophys. J.* 529, L45–L48.
- Charbonneau, D., Brown, T.M., Noyes, R.W., Gilliland, R.L., 2002. Detection of an extra-solar planet atmosphere. *Astrophys. J.* 568, 377–384.
- Cravens, T.E., 1987. Vibrationally excited molecular hydrogen in the upper atmosphere of Jupiter. *J. Geophys. Res.* 92, 11083–11100.
- Datz, S., Sundström, G., Biedermann, C., Brostrom, L., Danared, H., Mannervik, S., Mowat, J.R., Larsson, M., 1995. Branching processes in the dissociative recombination of H_3^+ . *Phys. Rev. Lett.* 74, 896–899.
- Goukenleuque, C., Bezaud, B., Joguet, B., Lellouch, E., 2000. A radiative equilibrium model of 51 Peg b. *Icarus* 143, 308–323.
- Guillot, T., Burrows, A., Hubbard, W.B., Lunine, J.I., Saumon, D., 1996. Giant planets at small orbital distances. *Astrophys. J.* 459, L35–L38.
- Ham, D.O., Trainor, D.W., Kaufman, F., 1970. Gas phase kinetics of $\text{H} + \text{H} + \text{H}_2 \rightarrow 2\text{H}_2$. *J. Chem. Phys.* 53, 4395.
- Henry, G.W., Marcy, G.W., Bulter, R.P., Vogt, S.S., 2000. A transiting “51 Peg-like” planet. *Astrophys. J.* 529, L41–L44.
- Hickey, M.P., Walterscheid, R.L., Schubert, G., 2000. Gravity wave heating and cooling in Jupiter’s thermosphere. *Icarus* 148, 266–281.
- Hubbard, W.B., Yelle, R.V., Lunine, J.I., 1990. Nonisothermal Pluto atmosphere models. *Icarus* 84, 1–11.
- Hummer, D.G., Seaton, M.J., 1963. The ionization structure of planetary nebulae. I. Pure hydrogen nebulae. *Mon. Not. R. Astron. Soc.* 125, 437–459.
- Hunten, D.M., 1982. Thermal and nonthermal escape mechanisms for terrestrial bodies. *Planet. Space Sci.* 30, 773–783.
- Hunten, D.M., Watson, A.J., 1982. Stability of Pluto’s atmosphere. *Icarus* 51, 665–667.
- Kapras, Z., Anicich, V.G., Huntress, W.T., 1979. An ion cyclotron resonance study of reactions of ions with hydrogen atoms. *J. Chem. Phys.* 70, 2877–2881.
- Kasting, J.F., Pollack, J.B., 1983. Loss of water from Venus. I. Hydrodynamic escape of hydrogen. *Icarus* 53, 479–508.
- Krasnopolsky, V.A., 1999. Hydrodynamic flow of N_2 from Pluto. *J. Geophys. Res.* 104, 5955–5962.
- Lammer, H., Selsis, F., Ribas, I., Guinan, E.F., Bauer, S.J., Weiss, W.W., 2003. Atmospheric loss of exoplanets resulting from stellar X-ray and extreme-ultraviolet heating. *Astrophys. J.* 598, L121–L124.
- Liang, M.-C., Parkinson, C.D., Lee, A.Y.-T., Yung, Y.L., Seager, S., 2003. Source of atomic hydrogen in the upper atmosphere of HD 209458b. *Astrophys. J.* 596, L247–L250.
- Lias, S.G., Bartmess, J.E., Liebman, J.F., Holmes, J.L., Levin, R.D., Mallard, W.G., 1988. Gas-phase ion and neutral thermochemistry. *J. Phys. Chem. Ref. Data* 17, 1–861.
- Majeed, T., McConnell, J.C., 1991. The upper ionospheres of Jupiter and Saturn. *Planet. Space Sci.* 39, 1715–1732.
- Majeed, T., Yelle, R.V., McConnell, J.C., 1991. Vibrationally excited H_2 in the outer planets thermosphere—fluorescence in the Lyman and Werner bands. *Planet. Space Sci.* 39, 1591–1606.
- Majeed, T., McConnell, J.C., Gladstone, G.R., 1999. A model analysis of Galileo electron densities on Jupiter. *Geophys. Res. Lett.* 26, 2335.
- Mason, E.A., Marrero, T.R., 1970. The diffusion of atoms and molecules. In: Bates, D.R., Estermann, I. (Eds.), *Advances in Atomic and Molecular Physics*. Academic Press, New York, pp. 155–232.
- Matcheva, K.I., Strobel, D.F., 1999. Heating of Jupiter’s thermosphere by dissipation of gravity waves due to molecular viscosity and heat conduction. *Icarus* 140, 328–340.
- Matcheva, K.I., Strobel, D.F., Flasar, F.M., 2001. Interaction of gravity waves with ionospheric plasma: implications for Jupiter’s ionosphere. *Icarus* 152, 347–365.
- Mayor, M., Queloz, D., 1995. A Jupiter-mass companion to a solar-type star. *Nature* 378, 355–359.
- McConnell, J.C., Majeed, T., 1987. H_3^+ in the jovian ionosphere. *J. Geophys. Res.* 92, 8570–8578.
- McNutt, R.L., 1989. Models of Pluto’s upper atmosphere. *Geophys. Res. Lett.* 16, 1225–1228.
- Müller-Wodarg, I.C.F., Yelle, R.V., Mendillo, M., Young, L.A., Aylward, A.D., 2000. The thermosphere of Titan simulated by a global three-dimensional time-dependent model. *J. Geophys. Res.* 105, 20833–20856.
- Neale, L.S., Miller, S., Tennyson, J., 1996. Spectroscopic properties of the H_3^+ molecule: a new calculated line list. *Astrophys. J.* 464, 516–520.
- Richardson, L.J., Deming, D., Wiedemann, G., Goukenleuque, C., Steyert, D., Harrington, J., Esposito, L.W., 2003. Infrared observations during the secondary eclipse of HD 209458b. I. 3.6 micron occultation spectroscopy using the very large telescope. *Astrophys. J.* 584, 1053–1062.
- Schauer, M.M., Jefferts, S.R., Barlow, S.E., Dunn, G.H., 1989. Reactions of H_2 with He^+ at temperatures below 40 K. *J. Chem. Phys.* 91, 4593–4596.
- Schubert, G., Hickey, M.P., Walterscheid, R.L., 2003. Heating of Jupiter’s thermosphere by the dissipation of upward propagating acoustic waves. *Icarus* 163, 398–413.
- Seager, S., Whitney, B.A., Sasselov, D.D., 2000. Photometric light curves and polarization of close-in extrasolar giant planets. *Astrophys. J.* 540, 504–520.
- Seaton, M.J., 1960. HI, HeI and HeII intensities in planetary nebulae. *Mon. Not. R. Astron. Soc.* 120, 326.
- Storey, P.J., Hummer, D.G., 1995. Recombination line intensities for hydrogenic ions. IV. Total recombination coefficients and machine-readable tables for $Z = 1$ to 8. *Mon. Not. R. Astron. Soc.* 272, 41–48.
- Sudarsky, D., Burrows, A., Hubeny, I., 2003. Theoretical spectra and atmospheres of extra-solar giant planets. *Astrophys. J.* 588, 1121–1148.
- Sundström, G., Mowat, J.R., Danared, H., Datz, S., Brostrom, L., Filevich, A., Kallberg, A., Mannervik, S., Rensfelt, K.G., Sigra, P., af Ugglas, M., Larsson, M., 1994. Destruction rate of H_3^+ by low-energy electrons measured in a storage ring experiment. *Science* 263, 785–787.
- Thread, L.P., Huntress, W.P., 1974. Ion molecules reactions and vibrational deactivation of H_2^+ ions in mixtures of hydrogen and helium. *J. Chem. Phys.* 60, 2840–2848.
- Vidal-Madjar, A., Lecavelier des Etangs, A., Desert, J.-M., Ballester, G.E., Ferlet, R., Hébrard, G.H., Mayor, M., 2003. An extended upper atmosphere around planet HD209458b. *Nature* 422, 143–146.
- Waite, J.H., Cravens, T.E., Kozyra, J., Nagy, A.F., Atreya, S.K., Chen, R.H., 1983. Electron precipitation and related aeronomy of the jovian thermosphere and ionosphere. *J. Geophys. Res.* 88, 6143–6163.
- Waite, J.H., Gladstone, G.R., Lewis, W.S., Drossart, P., Cravens, T.E., Maurellis, A.N., Mauk, B.H., Miller, S., 1997. Equatorial X-ray emissions: implications for Jupiter’s high exospheric temperatures. *Science* 276, 104–108.
- Watson, A.J., Donahue, T.M., Walker, J.C.G., 1981. The dynamics of a rapidly escaping atmosphere: application to the evolution of Earth and Venus. *Icarus* 48, 150–166.
- Wolven, B.C., Feldman, P.D., Strobel, D.F., McGrath, M.A., 1997. Ly alpha induced fluorescence of H_2 and CO in Hubble Space Telescope spectra of a Comet Shoemaker–Levy 9 impact site on Jupiter. *Astrophys. J.* 475, 835–842.
- Woods, T.N., Rottman, G.J., Bailey, S.M., Worden, J.R., 1998. Solar extreme ultraviolet irradiance measurements during solar cycle 22. *Sol. Phys.* 177, 133–146.
- Yan, M., Sadeghpour, H.R., Dalgarno, A., 1998. Photonization cross sections of He and H_2 . *Astrophys. J.* 496, 1044–1050.
- Yelle, R.V., Miller, S., 2004. The thermosphere and ionosphere of Jupiter. In: Bagenal, F., McKinnon, W., Bowling, T. (Eds.), *Jupiter: Planet, Satellites, and Magnetosphere*. Cambridge Univ. Press, Cambridge, pp. 000–001.
- Young, L.A., Yelle, R.V., Young, R.E., Sieff, A., Kir, D.B., 1997. Gravity waves in Jupiter’s thermosphere. *Science* 276, 108–111.
- Yousif, F.B., Mitchell, J.B.A., 1989. Recombination and excitation of HeH^+ . *Phys. Rev. A* 40, 4318–4321.